A Passive Variable Switching Frequency SPWM Concept and Analysis for DCAC Converter

Xiaonan Zhu, *Student Member, IEEE*, Hongliang Wang, *Senior Member, IEEE*, Wenyuan Zhang, Hanzhe Wang, Xiaojun Deng, Wei Tang, and Xiumei Yue

***Abstract*—Variable switching frequency sinusoidal pulsewidth modulation (VSFSPWM) method does well in many aspects such as lower harmonic peak and losses compared with constant switching frequency sinusoidal pulsewidth modulation (CSFSPWM) for DCAC converters. This article presents a passive VSFSPWM (PVSFSPWM) method for spectrum improvement, filter inductor reduction, and losses reduction, obtaining similar output current quality as that of the CSFSPWM method. Because the PVSFSPWM method does not need any feedback information compared with the model-predictive-based method, it is an open-loop method and is called the passive method. In order to obtain the law of harmonic distribution, the mathematical expression of harmonic spectrum distribution is derived. The required filter inductor under the same current ripple and the losses between CSFSPWM and PVSFSPWM methods have been compared. Simulation and experimental results show that the PVSFSPWM method achieves excellent performance in EMI suppression, inductance, and losses reduction without impairing the output quality.**

***Index Terms*—DCAC converter, pulsewidth modulation, variable switching frequency.**

I. Introduction

SINUSOIDAL pulsewidth modulation (SPWM), characterized by a rapid dynamic response, reducing the harmonics in a low-frequency band, and so on, is one of the most popular research topics in a DCAC power conversion with the application of the high-frequency, full-controlled switching devices [1]. It is widely used in photovoltaic (PV) inverters, wind converters, motor drivers, uninterruptible power supply, and other applications [2], [3].

For the constant switching frequency SPWM (CSFSPWM) method, the harmonics caused by the rapid turn-ON and turn-OFF switching devices will appear in the spectra at the switching frequency and its multiple frequencies, and it can arrive at a high amplitude [4]. The harmonics with high peak value will contribute to the electromagnetic interference (EMI), and it is harmful to the power electronic system [5]. In a motor drive system, the overvoltage caused by harmonics will reduce the insulation performance of the winding and the life of the motor [6]. In grid-connected applications, inverters should not inject excessive harmonic currents into the grid to ensure that no adverse effects are caused on other devices connected to the grid. The total harmonic distortion (THD) rate is limited to 5% and each order harmonic is strictly restricted [6].

In order to reduce the peak value of the harmonic, the variable switching frequency SPWM (VSFSPWM) method has become a research hotspot [7], [8]. Based on spread-spectrum SPWM techniques, some methods with remarkable effect are put forward in the past few years such as random SPWM (RSPWM) [9], [10], programmed SPWM (PSPWM) [11], [12], and chaotic SPWM (CSPWM) [13], [14]. The principle of RSPWM is that the switching frequency is changed from a fixed value into a continuous value in a certain range, the distribution of high-order harmonics also changes from discrete to continuous. As a result, the peak value of the spectrum is reduced. Although RSPWM has achieved good results, it is still faced with difficulties such as difficult to quantify, uncontrollable performance, and being implemented in the industry [15]. The programmed SPWM can eliminate specific harmonics, so it is also known as a selective harmonic elimination method. This method is attractive in a wide range of low switching frequencies. However, it is limited when dealing with a large number of harmonics due to complex online computing [16]. The mechanism of chaotic SPWM is similar to RSPWM. It can evenly distribute the harmonics in a wide frequency band so that some harmonics with larger amplitude can be effectively suppressed. However, this method consumes a lot of computing resources and has low computing speed, and it is difficult to generate chaotic sequences in real time [17].

In addition to the conventional methods, some advanced PWM technologies for power electronics converters have been proposed. With the target of ac-side current ripple, the model predictive PWM (MPP) is first proposed in single-phase inverters [18]. The ripple current variation in one switching cycle has been systematically researched in [19] and [20], and a current ripple prediction method through the Thevenin equivalent circuits is also given. Two MPPs techniques are proposed in [21] for three-phase motor drive applications. They not only arrange

Manuscript received May 31, 2021; revised September 7, 2021; accepted October 16, 2021. Date of publication October 27, 2021; date of current version January 19, 2022. This work was supported in part by the National Natural Science Foundation of China under Grant 51977069, in part by the Innovative Talents of "High-Level Talent Gathering Project" of Hunan Province, China, under Grant 2018RS3048, in part by the Natural Science Foundation for Distinguished Young Scholars of Hunan Province, China, under Grant 2020JJ2007, in part by the First Key Research and Talents Preprogram of Changsha, Hunan Province, China, under Grant kq2004020, and in part by the National Natural Science Foundation Youth Project of China under Grant 52107195. Recommended for publication by Associate Editor F. Gao. *(Corresponding author: Hongliang Wang.)*

The authors are with the College of Electrical and Information Engineering, Hunan University, Changsha 410082, China (e-mail: zhuxn@hnu.edu.cn; liangliang-930@163.com; wenyuanzhang@hnu.edu.cn; hanzhewang@hnu.edu.cn; xiaojundeng@hnu.edu.cn; weitang@hnu.edu.cn; yuexm@hnu.edu.cn).

Color versions of one or more figures in this article are available at https://doi.org/10.1109/TPEL.2021.3123190.

Digital Object Identifier 10.1109/TPEL.2021.3123190

peak or rms value of the current ripple within the required range but also reduce the average switching frequency and EMI noise effectively. A similar MPP strategy for dc-link voltage ripple reduction is proposed in [22]. All these current ripple prediction-based methods have done well in EMI and losses reduction. However, they belong to closed-loop methods, which means that some information such as switch status and duty cycle are required to obtain the switching cycle in every interrupt cycle. It will bring a heavy burden on the microprocessor especially when the vector increases. With the target of losses reduction, an optimal MPP is proposed in [23]. The average value of switching losses function over a whole period is given and the output current ripple rms value has been defined as a constraint. This method can reduce the switching losses by 19% compared with constant frequency PWM. However, the parameters of the objective function are acquired from a look-up table (LUT) and the data of the LUT are calculated offline using the toolbox of MATLAB, so it may be inconvenient in the industrial scene. Another method is proposed in [24]. It increases the switching frequency when the reference voltage approaches zero so that the current ripple can be reduced. However, there are no mathematical methods to quantify the performance of current ripple reduction, which means the performance is not controllable. Additional variable switching frequency methods have been proposed in [25]–[27] the motor-drive applications.

For these advanced PWM technologies, some information is required to calculate the switching cycle. Hence, they are called closed-loop methods. They only focus on the improvement of single performance such as current ripple or losses. And they also need complex online mathematical calculations. In this article, a PVSFSPWM method is proposed. First of all, the pulse signal is obtained by comparing sine wave and triangle wave, just like the CSFSPWM method, without complicated online calculation. Second, it can effectively reduce the harmonic peak as well as EMI. Third, the PVSFSPWM method needs smaller filter inductance than the CSFSPWM method under the same ripple current requirement. Finally, the losses of the PVSFSPWM method are smaller than that of the CSFSPWM method when proper parameters are selected. It should be noted that the PVSFSPWM method can be applied not only to single-phase systems but also to three-phase or even n-phase systems. Here, the single-phase system is taken as an example for a detailed analysis.

The rest of this article is organized as follows. In Section II, the principle of PVSFSPWM method is given. In Section III, the mathematical analysis of a harmonic spectrum is derived, and the required inductor and the losses between CSFSPWM and PVSFSPWM methods are compared. Section IV introduces the digital implementation. The effectiveness of the PVSFSPWM method is verified based on a full-bridge inverter in Section V. Finally, Section VI concludes this article.

II. Principle of the Proposed PVSFSPWM Method

A. Introduction of the Proposed PVSFSPWM Method

Fig. 1 shows the modulation strategies for both CSFSPWM and PVSFSPWM methods. The red line (u_r) is a reference sinusoidal wave and T is a power line period. The dark blue line

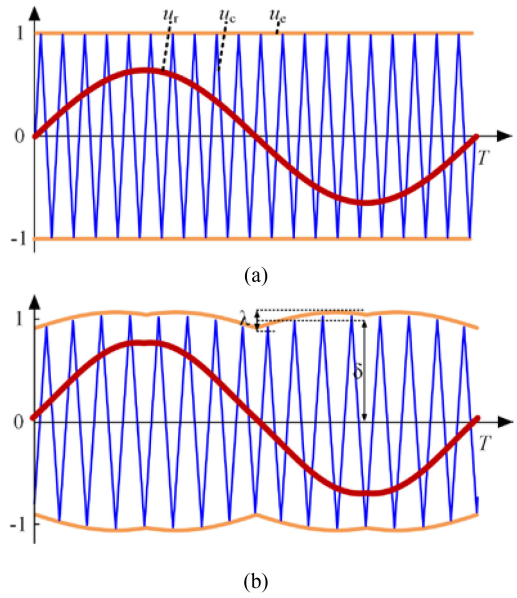

Fig. 1. Modulation strategy comparison. (a) CSFSPWM method. (b) Proposed PVSFSPWM method.

(u_c) is a carrier wave and the orange line (u_e) is the envelope of the triangular carrier amplitude. For the CSFSPWM method in Fig. 1(a), u_e is constant and it can be equivalent to a periodic function with an infinite period. Thus, the switching period is constant. For the PVSFSPWM method as shown in Fig. 1(b), it can be regarded that u_e is injected into the amplitude of the carrier, so the frequency varies with u_e. u_e needs to satisfy the following constraints.

1) u_e is a periodic function with a period of $T/2$.
2) u_e is preferably even symmetry within a power line period; it is beneficial to eliminate harmonics.
3) u_e and u_r have the same phase angle.

Different from the MPP methods, the switching period is obtained naturally rather than by a complex mathematical prediction method. Therefore, the PVSFSPWM method is opened and it is also called passive. In addition, the performance of the PVSFSPWM method can be accurately evaluated.

The different performances will be achieved when different u_e is selected. In order to quantify the influence of injection function parameters on the system performance, the injection depth D (λ, δ) for the injected function is defined here. The parameter λ is the peak-to-peak value of u_e and δ is the overall bias of u_e. Obviously, the larger λ is, the wider the range of switching frequency variation is; the larger δ is, the smaller the average frequency is. In other words, the distribution of the spectrum and the value of switching losses are directly related to the injection depth D.

B. Mathematical Analysis of the PVSFSPWM Method

The carrier triangular of the PVSFSPWM method in a switching cycle is illustrated in Fig. 2. The triangular OAB is the constant frequency carrier with a unit amplitude and its period is a. The triangular OCD is the variable frequency carrier with an amplitude of k. Because the switching frequency is high

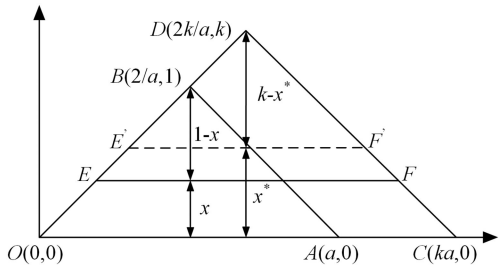

Fig. 2. Carrier triangular in a switching period.

enough compared with the reference frequency, the reference in a switching cycle is constant, which is marked with *EF*. *OAB* and *OCD* have the same slope but different amplitudes, as a result, the frequency is different.

In the cartesian coordinates, the coordinate origin is $O(0, 0)$, the height of *OAB* is unit, and the length of the line segment *OA* is a, then points *A* and *B* can be expressed as $(a,0)$ and $(2/a,1)$. Furthermore, the OFF-state duty cycle D_{off} can be calculated with (1), here D_{off} is defined as the ratio of turn-OFF time to a switching cycle in *OAB*. If the height is extended by a factor of k, points *C* and *D* can be expressed as $(ka, 0)$ and $(2k/a, k)$ according to the triangle similarity theorem. Finally, D_{off} in *OCD* can be calculated in (2)

$$D_{\text{off}} = 1 - x \tag{1}$$

$$D_{\text{off}} = (k - x)/k. \tag{2}$$

Comparing (1) and (2), D_{off} is different by using the constant slope carrier triangular. Thus, some distortion will appear in the output voltage and current. In order to make the output consistent with the input, the reference needs to be compensated. Supposing the new reference is *E'F'* and its value is x^*, combining (1) and (2), the new reference value x^* is achieved with (3). The same duty cycle as the CSFSPWM method will be achieved when x^* is adopted

$$x^* = kx. \tag{3}$$

Equation (3) shows that the amplitude of the triangle carrier and the amplitude of the sinusoidal modulation wave are increased or decreased by k times at the same time to obtain the same duty cycle in each switching period, so there is no overmodulation issue.

C. Other Typical Implementations

As discussed earlier, u_{e} is a function with periodicity and symmetry characteristics. Fig. 3 shows some detailed implementations. In Fig. 3(a) and (b), u_{e} is a triangle wave, and their injection depths are $D(0.2, 1)$ and $D(-0.2, 1)$, respectively. Similarly, a sine wave can be injected into the carrier as shown in Fig. 3(c) and (d), and their injection depths also are $D(0.2, 1)$ and $D(-0.2, 1)$, respectively. Here, the triangular wave injection method is illustrated in this article and the analytical methods for other methods are the same.

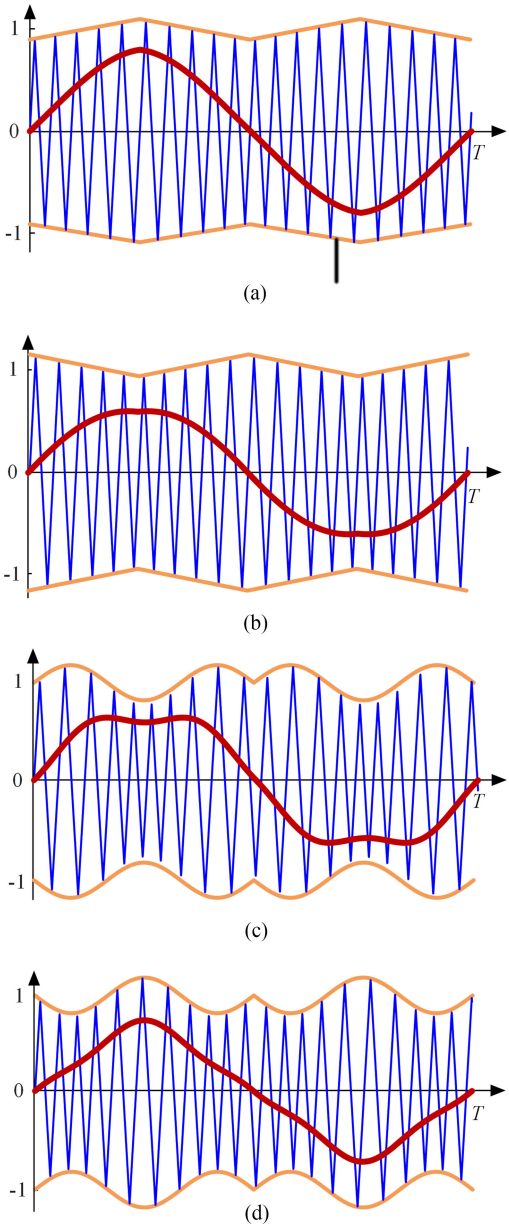

Fig. 3. Some typical implementations. (a) Inverse triangular wave injection. (b) In-phase sine wave injection. (c) Inverse-phase sine wave injection.

III. Comprehensive Analysis

A. Harmonic Spectrum Distribution Analysis

Before analyzing the spectrum of the PVSFSPWM method, it is better to overview the spectrum analysis method for the CSFSPWM method. Usually, the regular time-varying waveform can be expressed as an infinite Fourier series based on the Fourier transform. For a signal that is a dual function of two variables, the double Fourier series has been introduced to analyze the spectrum over the past few decades [28].

Consider a dual function $f(x(t), y(t))$, where $x(t)$ and $y(t)$ are two periodic functions, the double Fourier series can be expressed with (4) according to the double Fourier series theory [28]. m is the index variable of carrier harmonic and n is the index

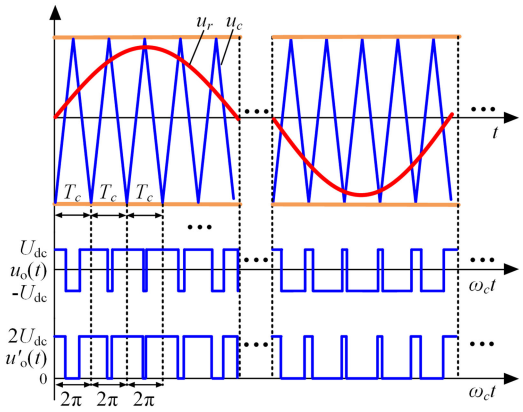

Fig. 4. Modulation principle of the CSFSPWM method.

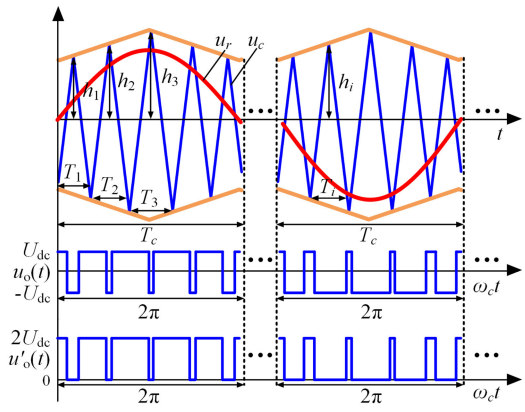

Fig. 5. Modulation principle of the PVSFSPWM method.

variable of baseband harmonic. $A_{\rm mn}$ and $B_{\rm mn}$ are the Fourier coefficients

$$\begin{aligned} f(t) &= f(x,y) \\ &= \frac{A_{00}}{2} + \sum_{n=1}^{\infty}[A_{0n}\cos ny + B_{0n}\sin ny] \\ &\quad + \sum_{m=1}^{\infty}[A_{m0}\cos mx + B_{m0}\sin mx] \\ &\quad + \sum_{m=1}^{\infty}\sum_{\substack{n=-\infty \\ n\neq 0}}^{\infty}\{A_{mn}\cos[mx+ny] \\ &\quad + B_{mn}\sin[mx+ny]\} \end{aligned} \tag{4}$$

where

$$A_{mn} + jB_{mn} = \frac{1}{2\pi^2}\int_{-\pi}^{\pi}\int_{-\pi}^{\pi} f(x,y)e^{j(mx+ny)}dxdy. \tag{5}$$

Fig. 4 shows the modulation principle of the CSFSPWM method. $U_{\rm dc}$ is the input dc voltage. $u_{\rm o}(t)$ is the output PWM voltage. $T_{\rm c}$ is the period of the carrier. When $u_{\rm r}$ is greater than $u_{\rm c}$, $u_{\rm o}(t) = U_{\rm dc}$, otherwise $u_{\rm o}(t) = -U_{\rm dc}$. In order to simplify the calculation, a dc component $U_{\rm dc}$ is added to $u_{\rm o}(t)$ to get a new output voltage $u'_o(t)$. $u'_o(t)$ switches between 0 and $2U_{\rm dc}$, whereas the harmonic distribution is the same as that of $u_{\rm o}(t)$. Then, $u'_o(t)$ can be written as a double Fourier series of $x(t)$ and $y(t)$ as shown in (6) and (7). Hereafter, ω_c is carrier angular frequency, θ_c is a phase offset angle of a carrier, ω_r is the reference angular frequency, and θ_r is a phase offset angle of the reference

$$u'_{\rm o}(t) = u_{\rm o}(x,y) \tag{6}$$

$$\begin{aligned} x(t) &= \omega_c t + \theta_c \\ y(t) &= \omega_r t + \theta_r \end{aligned} \tag{7}$$

$$\begin{aligned} u'_{\rm o}(t) &= \{U_{\rm dc} + MU_{\rm dc}\cos(\omega_r t + \theta_r)\} \\ &\left\{-\frac{4U_{\rm dc}}{m\pi}\sum_{m=1}^{\infty} J_0\left(\frac{mM\pi}{2}\right)\sin\left(m\frac{\pi}{2}\right)\cos[m(\omega_c t+\theta_c)]\right\} \\ &\left\{-\frac{4U_{\rm dc}}{m\pi}\sum_{m=1}^{\infty}\sum_{\substack{n=-\infty \\ n\neq 0}}^{\infty} J_n\left(\frac{mM\pi}{2}\right)\sin\left[(m-n)\frac{\pi}{2}\right] \right. \\ &\left. \times\cos[m(\omega_c t+\theta_c)+n(\omega_r t+\theta_r)]\right\}. \end{aligned} \tag{8}$$

Combining (6) and (7), the expression of a harmonic component for $u'_o(t)$ can be derived with (8). M is the injection depth and $J_{\rm n}$ is the Bessel function. The first item is the dc component of $U_{\rm dc}$; the second item is the fundamental component and its baseband harmonic component; the third item is the carrier harmonic component; the fourth item is the sideband harmonic component.

Generally, it is difficult to apply the double Fourier analysis method to the VSFPWM method because the carrier is aperiodic. However, when the carrier period varies in multiple cycles according to a predetermined value, the mathematical method for harmonic spectrum calculation still can be obtained [29], [30]. For the PVSFSPWM method, the mathematical calculation method for harmonic spectrum is theoretically available because the injected function is periodic.

Fig. 5 shows the modulation principle for the PVSFSPWM method. To obtain the double Fourier series of $u'_o(t)$, the period of the entire varying carrier is defined as $T_{\rm c}$, which includes k switching cycles. Here, T_i (i = 1,2,…,k) is the period of each carrier, and h_i is the height of each carrier. Because the frequency of $u_{\rm e}$ is two times of the power line frequency, $T_{\rm c}$ is equal to $T/2$. At the same time, it is necessary to convert the horizontal ordinate to $x = \omega_c t$, where $\omega_c = 2\pi/T_c$. Finally, the period of the variable carrier is converted to 2π.

According to the double Fourier analysis method of aperiodic carrier modulation, the mathematical expression of a harmonic component for $u'_o(t)$ under the PVSFSPWM method is derived with (9). It can be observed from (9) that the dc component and the fundamental component of the PVSFSPWM method are the same as those of the CSPWM method. For example, the dc component is $U_{\rm dc}$ and the amplitude of the fundamental component is $MU_{\rm dc}$. However, the distribution of the carrier

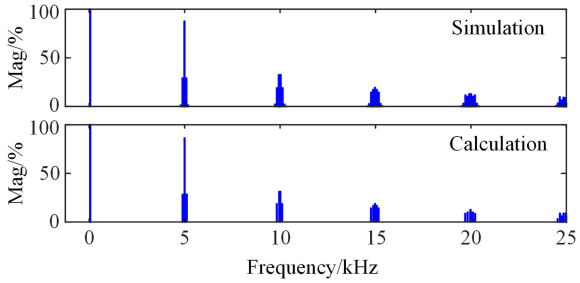

Fig. 6. Simulation and calculation results of the FFT analysis for output PWM voltage with $D(0, 1)$.

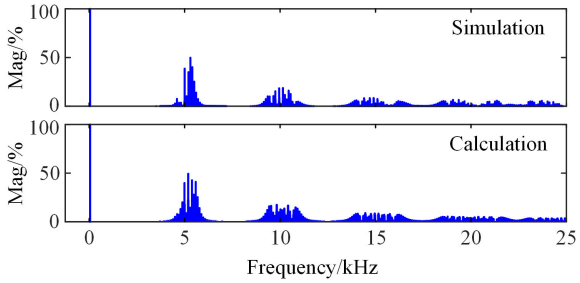

Fig. 7. Simulation and calculation results of the FFT analysis for output PWM voltage with $D(0.2, 1)$.

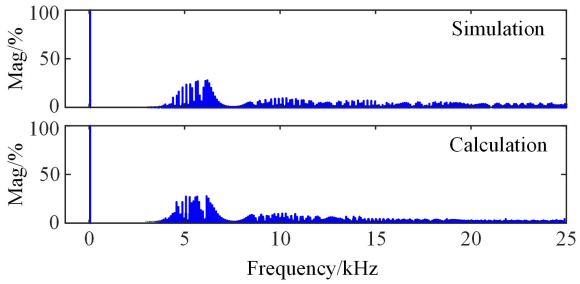

Fig. 8. Simulation and calculation results of the FFT analysis for output PWM voltage with $D(0.5, 1)$.

harmonics and the sideband harmonics for the two methods are different. The carrier harmonics and the sideband harmonics are not only related to the variable carrier period T_i but also related to the sum of the carrier period T_c. They are distributed in the frequencies of $m\omega_c$ and $m\omega_c+n\omega_r$, so the harmonics distribute at more frequency points and broader frequency bands. As long as M and $U_{\rm dc}$ are constant, the THD of power converters under both CSFSPWM and VSFPWM methods are equal [29]. Therefore, the peak value of the harmonic will be greatly reduced.

In order to verify the effectiveness of the mathematical analysis method, a comparison between simulation results and mathematical calculation results has been made. Figs. 6 –9 show the FFT results of the output PWM voltage under different injection depths. It is observed that the simulation results of the harmonic spectrum are consistent with the theoretical calculation results. With the increase of λ, the harmonic will be distributed in more frequencies, and the peak value of the harmonic is greatly reduced. Equation (9) is at the bottom of the next page.

Fig. 10 shows the simulation results of EMI comparison. The PVSFSPWM method with the injection depth $D(0.8, 1)$ and

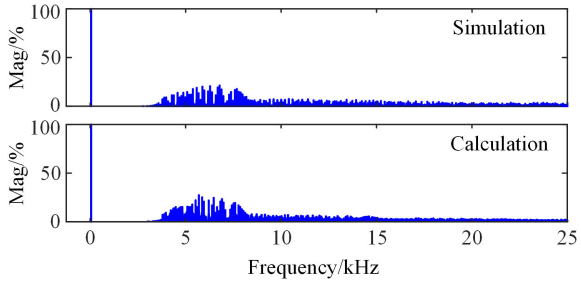

Fig. 9. Simulation and calculation results of the FFT analysis for output PWM voltage with $D(0.8, 1)$.

the CSFSPWM method with the fixed switching frequency are compared. It can be seen that the EMI of the CSFSPWM method presents periodic peaks in the frequency domain according to the integral multiple of the switching frequency. The EMI oscillation amplitude of the PVSFSPWM method is smaller and a reduction of about 30 dB can be achieved. In summary, the average energy of the two methods is similar, but the peak value of EMI of the PVSFSPWM method is much smaller than that of the CSFSPWM method.

B. Current Ripple Reduction Analysis

Because the slope of each triangle is equal, the period of the carrier triangle is proportional to the height. Supposing the basic frequency is f_b, the switching frequency for each carrier triangle under the PVSFSPWM method is expressed as (10). Obviously, the frequency of each carrier varies around f_b, and the CSFSPWM method is a special case of the PVSFSPWM method when the injection depth is $D(0, 1)$

$$f_i = \frac{f_b}{h_i}. \tag{10}$$

The average switching frequency during a power line period can be derived as

$$f_{\rm avg} = \frac{f_b}{\lambda} \ln\left(\frac{2\delta+\lambda}{2\delta-\lambda}\right). \tag{11}$$

The two-level voltage source inverter is taken as an example; the maximum current ripple ($\Delta I_{\rm max}$) of the inductor under the CSFSPWM method occurs when the phase angle is 0 and π, and it is written as (12). For the PVSFSPWM method, the maximum current ripple is written as (13)

$$\Delta I_{\rm max} = \frac{V_{\rm dc}T}{4L} \tag{12}$$

$$\Delta I_{\rm max} = \frac{V_{\rm dc}T}{4L}\left(\delta - \frac{\lambda}{2}\right). \tag{13}$$

Under the same requirement of peak ripple current, the ratio relationship of filter inductors of the two methods is shown in Fig. 11. The ratio m is defined as the ratio of the inductance under the VSFPWM method to that under the CSFSPWM method. It can be seen that m is directly proportional to δ and inversely proportional to λ. Detailly, with the increase of δ, the average switching frequency is reduced and the required filter inductor is increased in order to maintain the same peak ripple current. With

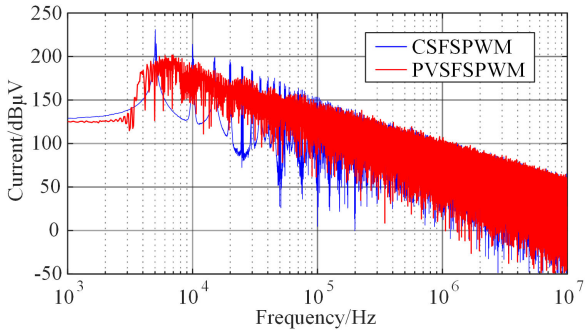

Fig. 10. Simulation results of EMI comparison.

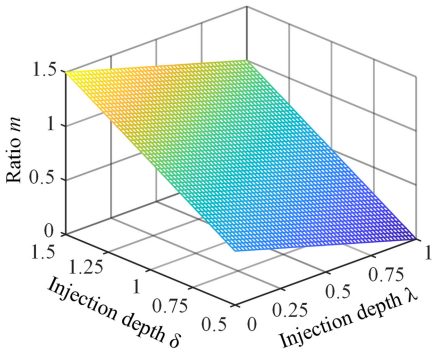

Fig. 11. Filter inductance comparison between PVSFSPWM and CSFSPWM methods under different injection depths.

the increase of λ, the average switching frequency is increased and the required filter inductor is decreased. Because the influence of δ and λ on the average switching frequency is different, the filter inductance and the average switching frequency can be reduced at the same by reasonably selecting the injection depth.

Fig. 12 shows the simulation results of the current ripple for both the CSFSPWM and the PVSFSPWM methods. Here, f_b is 5kHz, $\Delta I_{\max}$ is limited within 2 A. The other parameters are the same as those listed in Table I. Fig. 12(a) shows the current ripple for the CSFSPWM method. In order to limit $\Delta I_{\max}$ within 2 A, a 6.2-mH inductor is selected. It can be seen that the peak valley value of the amplitude envelope is quite different, so the utilization rate of switching frequency is low. Fig. 12(b) shows

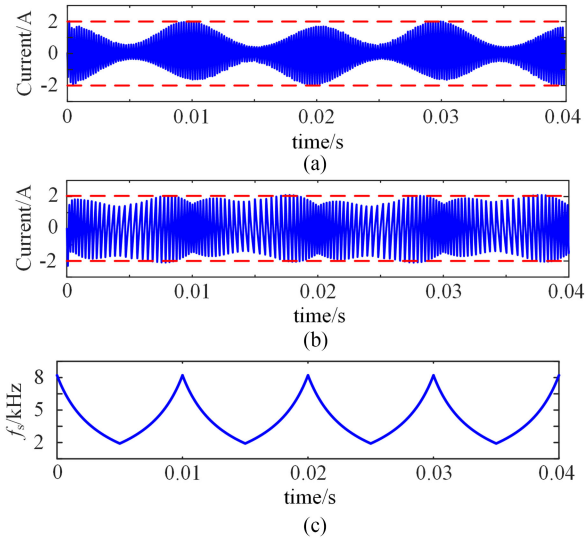

Fig. 12. Current ripple comparison between two methods. (a) Current ripple of the CSFSPWM method. (b) Current ripple of the PVSFSPWM method. (c) Switching frequency variation for the PVSFSPWM method.

TABLE I
COMPARISON WITH SOME EXISTING VSFSPWM METHODS

Methods	Classification	Controllable	Online calculation
RSPWM [9]	Passive	No	No
PSPWM [11]	Active	Yes	Yes
CSPWM [13]	Passive	No	No
[21]	Active	Yes	Yes
[23]	Active	Yes	Yes
PVSFSPWM	Passive	Yes	No

the current ripple for the PVSFSPWM method. The injection depth is D(1,1.2) and the inductor is 4.8 mH. Obviously, the current ripple distribution is greatly improved. The switching frequency varies from 2.8 to 8.2 kHz as shown in Fig. 12(c) and the average switching frequency reduces to 4.43 kHz. When f_b is equal to the frequency of the CSFSPWM method, the PVSFSPWM method can not only reduce the current ripple but also make the ripple more uniform. In other words, on the premise of meeting the peak–peak current standard, the PVSFSPWM method can reduce the filter inductor and the average switching frequency.

$$
\begin{aligned}
u_{\mathrm{o}}'(t) &= \{U_{\mathrm{dc}} + MU_{\mathrm{dc}}\cos(\omega_r t + \theta_r)\} \\
&\left\{ -\frac{4U_{\mathrm{dc}}}{m\pi}\sum_{m=1}^{\infty}\sum_{i=1}^{k}\left\{\left[\sin\left(m\frac{T_i}{4}\right)\cos m\left(\sum_{j=1}^{i-1}T_j+\frac{T_i}{2}\right)\right]J_0\left(\frac{mMT_i}{4}\right)\cos\left[m\left(\omega_c t+\theta_c\right)\right]\right\}\right. \\
&\left.\left\{ -\frac{4U_{\mathrm{dc}}}{m\pi}\sum_{m=1}^{\infty}\sum_{i=1}^{k}\left\{\left[\sin\left(m\frac{T_i}{4}\right)\sin m\left(\sum_{j=1}^{i-1}T_j+\frac{T_i}{2}\right)\right]J_0\left(\frac{mMT_i}{4}\right)\sin\left[m\left(\omega_c t+\theta_c\right)\right]\right\}\right\} \\
&\left\{ +\frac{4U_{\mathrm{dc}}}{m\pi}\sum_{m=1}^{\infty}\sum_{\substack{n=-\infty\\ n\neq 0}}^{\infty}\sum_{i=1}^{k}\left\{\left[\sin\left(\frac{n\pi}{2}-\frac{mT_i}{4}\right)\cos m\left(\sum_{j=1}^{i-1}T_j+\frac{T_i}{2}\right)\right]J_n\left(\frac{mMT_i}{4}\right)\cos\left[m(\omega_c t+\theta_c)+n(\omega_r t+\theta_r)\right]\right\}\right. \\
&\left.\left\{ +\frac{4U_{dc}}{m\pi}\sum_{m=1}^{\infty}\sum_{\substack{n=-\infty\\ n\neq 0}}^{\infty}\sum_{i=1}^{k}\left\{\left[\sin\left(\frac{n\pi}{2}-\frac{mT_i}{4}\right)\sin m\left(\sum_{j=1}^{i-1}T_j+\frac{T_i}{2}\right)\right]J_n\left(\frac{mMT_i}{4}\right)\sin\left[m(\omega_c t+\theta_c)+n(\omega_r t+\theta_r)\right]\right\}\right\}
\end{aligned}
\tag{9}
$$

C. Conduction and Switching Losses Analysis

The total losses of the switches mainly include conduction losses and switching losses. Generally, the conduction loss in the ith period $P_{\rm con}(i)$ can be written as

$$P_{\rm con}(i) = u_{\rm ce}(i) i_{\rm o}(i) D(i) \tag{14}$$

where $u_{\rm ce}(i) = U_{\rm ceo} + |i_{\rm o}(i)| R_{\rm T}$, $i_{\rm o}(i) = I_{\rm m} \sin(\omega_r \Delta i)$, and $I_{\rm m}$ is the peak value of the output current, $U_{\rm ceo}$ is the saturation voltage drop and $R_{\rm T}$ is the forward ON-resistance of IGBTs. $D(i)$ is the duty cycle as shown in (15), and Δi is the accumulation of switching periods before the ith period. For the PVSFSPWM method, it is obtained with (16)

$$D(i) = \frac{1 + M \sin(\omega_r \Delta_i)}{2} \tag{15}$$

$$\Delta_i = T_1 + T_2 + \cdots + T_{i-1} + T_i/2 \tag{16}$$

$$P_{\rm con} = \frac{2}{T} \sum_{i=1}^{N/2} \begin{bmatrix} \frac{U_{\rm ceo} I_{\rm m}}{2} \sin(\omega_r \Delta_i) T_i \\ + \frac{R_T I_{\rm m}^2 + M U_{\rm ceo} I_{\rm m}}{2} \sin^2(\omega_r \Delta_i) T_i \\ + \frac{M R_T I_{\rm m}^2}{2} \sin^3(\omega_r \Delta_i) T_i \end{bmatrix}. \tag{17}$$

The conduction losses during a whole power line period for an IGBT are expressed by the sum of the losses in all these switching periods as shown in (17). N is the total number of switching cycles in a power line period. Seen from (17), the integrals of function $\sin(\omega_r \Delta i) T_i$, $\sin^2(\omega_r \Delta i) T_i$, and $\sin^3(\omega_r \Delta i) T_i$ during a half-power period are fixed values. Therefore, $P_{\rm con}$ is the same for the CSFSPWM method and the PVSFSPWM method as long as $I_{\rm m}$ is the same.

The switching losses mainly include turn-ON loss and turn-OFF losses, they are proportional to the collector current. Here, the relationship curves between turn-ON energy ($E_{\rm on}$), turn-OFF energy ($E_{\rm off}$), and the collector current from the datasheet are used for switching losses calculation. The average switching loss $P_{\rm sw}$ in a switching period is written with

$$P_{\rm sw}(i) = \frac{(E_{\rm on}(i) + E_{\rm off}(i))}{T_i} \tag{18}$$

where $E_{\rm on}(i)$ and $E_{\rm off}(i)$ are expressed by (19). k_1, k_2 b_1, and b_2 are fitting coefficients. Based on (18) and (19), the total switching loss $P_{\rm sw}$ in an entire power line period is written as (20). It is obvious that $P_{\rm sw}$ depends on N. When the average frequency declines, the total $P_{\rm sw}$ will decline, meanwhile

$$\begin{aligned} E_{\rm on}(i) &= k_1 i_{\rm o}(i) + b_1 \\ E_{\rm off}(i) &= k_2 i_{\rm o}(i) + b_2 \end{aligned} \tag{19}$$

$$P_{\rm sw} = \frac{2}{T} \sum_{i=1}^{N/2} [(k_1 + k_2) I_{\rm m} \sin(\omega_r \Delta_i) + b_1 + b_2]. \tag{20}$$

Fig. 13 shows the losses distribution with different switching frequencies based on (17) and (20). Here, $P_{\rm con\_CSFSPWM}$ and $P_{\rm sw\_CSFSPWM}$ are the conduction and switching losses of an IGBT under the CSFSPWM method respectively, and $P_{\rm con\_PVSFSPWM}$ and $P_{\rm sw\_PVSFSPWM}$ are the conduction and switching losses under the PVSFSPWM method, respectively. The injection depth $D(1.2, 1)$ is selected as an example. It can be observed that the conduction losses of the two methods are almost the same while the switching losses under the PVSFSPWM method are less than that under the CSFSPWM method. Specifically, the switching losses of the PVSFSPWM method are about 30% less than that of the CSFSPWM method at all switching frequencies.

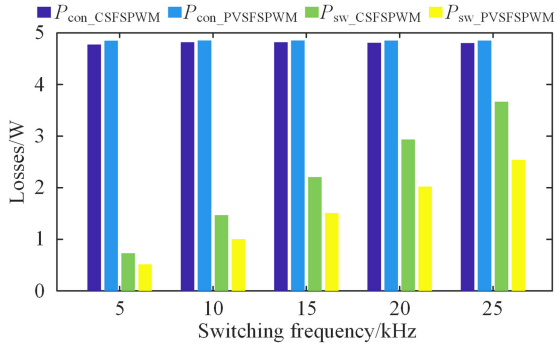

Fig. 13. Losses distribution with different switching frequencies.

D. Comparison With Some Existing VSFSPWM Methods

Table I gives a comparison between the PVSFSPWM method and some existing VSFSPWM methods. These methods can be roughly divided into active and passive. For PSPWM [11] and VSFSPWMs in [21] and [23], they are all active methods. They all require complex online calculations. For example, PSPWM needs to calculate the peak value of a specific subharmonic, and the methods in [21] and [23] need to calculate the current ripple. As the complexity of the system increases, the calculations will increase exponentially, which will bring a heavy burden to the microprocessor. For RSPWM [9], CSPWM [13], and the PVSFSPWM method, they are all passive methods without complex online calculation and feedback control, and they are easy to be implemented in a microprocessor. However, their effect is not as excellent as the active method. Among these passive methods, the PVSFSPWM method is superior to other methods in terms of controllability. This is because the PVSFSPWM method can adjust parameters such as spectrum distribution, current ripple, and loss through the injection depth while RSPWM and CSPWM methods are uncontrollable.

IV. Digital Realization

The digital realization of the PVSFSPWM method in the controller is presented in this section. Like the conventional CSFSPWM method, the PVSFSPWM method can also be realized by comparing a modulation wave with a carrier wave. As for the digital controller, it can be a digital signal processing (DSP) or a field-programmable gate array (FPGA).

In the DSP controller, the reference $u_{\rm r}$ and injected waves $u_{\rm e}$ are sampled when the value of the counter is equal to 0 as shown in Fig. 14. The period of carrier triangle wave at different positions is different, and the reference wave is sampled synchronously, which ensures that the duty cycle remains unchanged in each switching period and realizes regular sampling. The PWM is generated by the enhanced pulsewidth modulation (ePWM) module of DSP. The interrupt is triggered when the

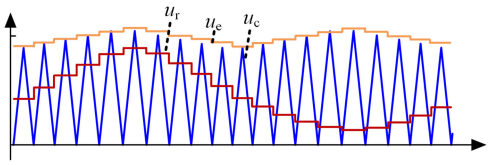

Fig. 14. Sampling reference and carrier waves in a DSP controller.

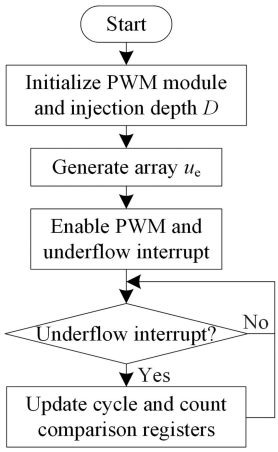

Fig. 15. Flowchart of the PVSFSPWM method in the DSP controller.

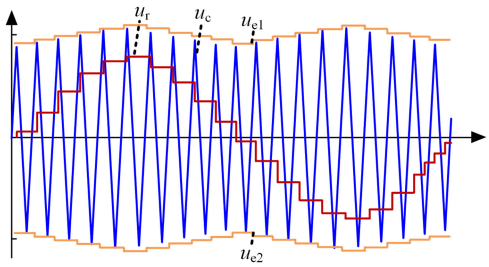

Fig. 16. Sampling reference and carrier waves in an FPGA controller.

value of the counter is zero. In the interrupt program, u_e is sent to the cycle register and the modulation sine wave is sent to the count comparison register.

The flowchart of the PVSFSPWM method in the DSP controller is shown in Fig. 15. First, it is necessary to initialize the ePWM module and the injection depth D. Second, the injected wave u_e is obtained and saved in an array according to the injection depth D. Third, the ePWM module and the underflow interrupt module are enabled. And then, the cycle register and count comparison register are updated in each interrupt.

In the FPGA controller, the sampling reference and carrier waves are shown in Fig. 16. Two waves u_{e1} and u_{e2} whose frequency is twice the reference wave frequency are generated in the controller. Their amplitude and offset are determined by the injection depth D. The counter is first set to increment. When the value of the counter increases to u_{e1}, set the counter to decrease; when the count value decreases to u_{e2}, set the counter to increment. After that, it keeps cycling. In this way, a carrier with variable frequency can be generated. The PWM signal can be obtained by comparing the modulated wave with the carrier wave.

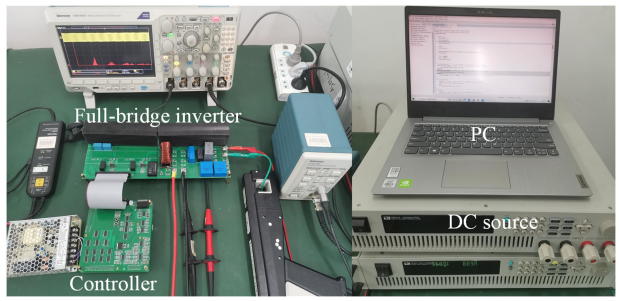

Fig. 17. Experimental hardware platform.

TABLE II
SYSTEM PARAMETERS

Parameters	Values	Parameters	Values
Input DC voltage	360 V	Output AC voltage	220 V / 50 Hz
Power rating	1 kW	Switching frequency	10 kHz
Output filter inductor	4 mH	Output filter capacitor	4.7 uF

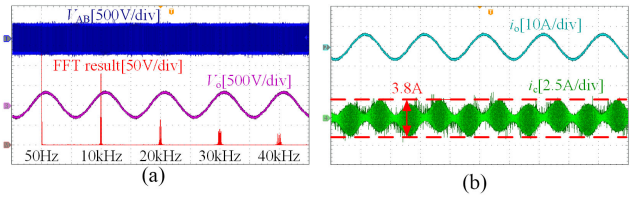

Fig. 18. Waveforms of the CSFSPWM method. (a) FFT result of bridge voltage V_{AB}. (b) Output current i_o and filter inductor ripple current i_c.

Comparing Figs. 14 and 16, there are more degrees of freedom to generate the carrier triangle in an FPGA controller, so the waveform consistent with the theoretical analysis can be achieved. However, the final effect of these two methods is completely the same because the changing law of the switching frequency is the same.

V. EXPERIMENTAL VERIFICATION

In this section, both the CSFSPWM and PVSFSPWM methods are verified based on a full-bridge inverter platform for comparison as shown in Fig. 17. They are implemented in the digital processor TMS320F28335 of Texas Instruments Incorporated. The parameters are reported in Table II. In the following, a number of experiments are carried out under different injection depths.

Fig. 18 shows the experimental results with the CSFSPWM method. Fig. 18(a) shows bridge voltage V_{AB}, output ac voltage V_o, and the FFT result of V_{AB}. In this situation, the switching frequency is constant; thus, the peak value of harmonics is mainly concentrated in the switching frequency and its integer multiple frequency. It is observed that the maximum peak value of the harmonic is almost 150 V. Fig. 18(b) shows the output current i_o and the filter inductor ripple current i_c. It can be seen that i_c reaches the maximum value at 0 and π, and it reaches the minimum value at $\pi/2$ and $3\pi/2$. The maximum peak–peak value is about 3.8 A.

Figs. 19 –21 show the experimental results with the PVSFSPWM method under different injection depths. Fig. 19 shows

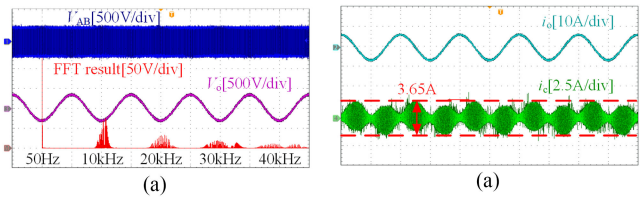

Fig. 19. Waveforms of the PVSFSPWM method under D(0.2, 1). (a) FFT result of bridge voltage V_{AB}. (b) Output current i_o and ripple current i_c.

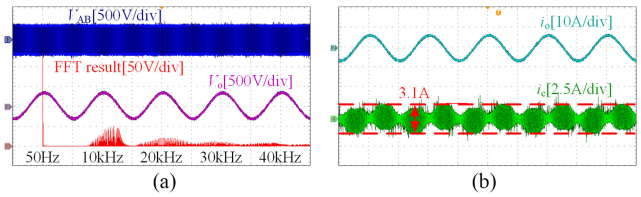

Fig. 20. Waveforms of the PVSFSPWM method under D(0.5, 1). (a) FFT result of bridge voltage V_{AB}. (b) Output current i_o and ripple current i_c.

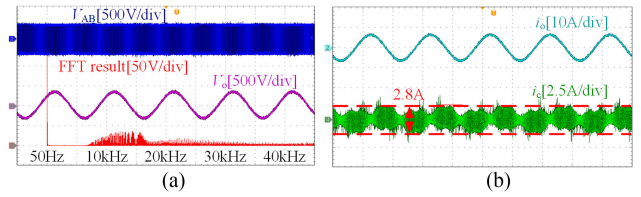

Fig. 21. Waveforms of the PVSFSPWM method under D(0.8, 1). (a) FFT result of bridge voltage V_{AB}. (b) Output current i_o and ripple current i_c.

the experimental results under D(0.2, 1). The switching frequency varies from 9.1 to 11.1 kHz. The peak value of the harmonics at the switching and its multiple frequencies has declined by 40% as shown in Fig. 19(a). In Fig. 19(b), the ripple current decreases to 3.65 A. Fig. 20 shows the experimental results under D(0.5, 1). In the circumstances, the switching frequency varies from 8 to 13.3 kHz. The peak value of the harmonics has declined by 60%, and the spectrum is smoother as shown in Fig. 20(a). As shown in Fig. 20(b), the ripple current decreases to 3.1 A. Fig. 21 shows the experimental results under D(0.8, 1). As shown in Fig. 21(a), the switching frequency varies from 7.1 to 16.6 kHz. The spectrum becomes continuous, and there are almost no peak values as can be seen. The peak value of the ripple current is only 2.8 A, so the current ripple is reduced by nearly 26% compared with the CSFSPWM method.

It can be also seen that from the experimental tests that, when δ is constant, the bigger λ is, the better the effect will be achieved. However, δ and λ have a deep relationship with the equivalent switching frequency f_{avg} from (11), and the switching losses will be increased with the increase of equivalent switching frequency. Therefore, it is better to consider the harmonic spectrum, the current ripple reduction, and the average switching frequency reduction to select a reasonable injection depth. These studies will be carried out in the future work in detail.

Fig. 22 shows the experimental results under D(1, 1.2). The switching frequency varies from 5.8 to 14.2 kHz and the average switching frequency is 8.8 kHz. The peak value of the ripple current is 3.5 A. Compared with the CSFSPWM method, the

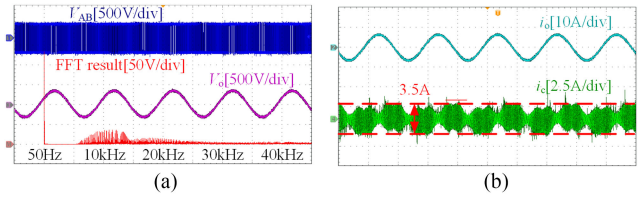

Fig. 22. Waveforms of the PVSFSPWM method under D(1, 1.2). (a) FFT result of bridge voltage V_{AB}. (b) Output current i_o and ripple current i_c.

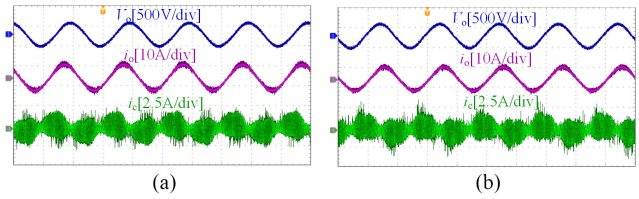

Fig. 23. Waveforms of the PVSFSPWM method under different PFs under D(1, 1.2). (a) Leading PF load (PF $= -0.82$). (b) Lagging PF load (PF $= 0.9$).

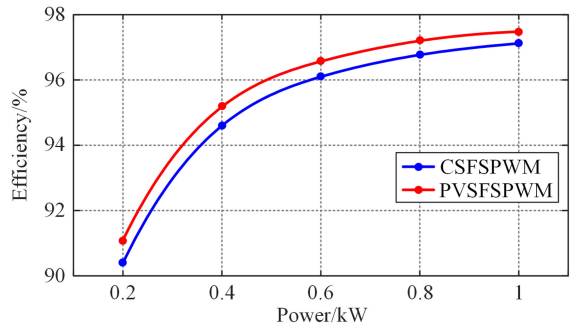

Fig. 24. Measured efficiency curves.

average switching frequency reduced by about 12%, and the current ripple reduced by about 8%.

To verify the reactive operation capability, experiments under different power factor (PFs) conditions are carried out under D(1, 1.2). Fig. 23(a) and (b) shows the experimental results under the leading PF condition and lagging PF condition, respectively. The power factor in Fig. 23(a) is -0.82 (capacitive), and in Fig. 23(b) is 0.9 (inductive). It can be seen that the peak-to-peak value of ripple currents is within 3.5 A.

By the power analyzer (HIOKI 3390), the measured efficiency of both CSFSPWM and PVSFSPWM methods are shown in Fig. 24. The injection depth for the PVSPWM method is D(1, 1.2). As seen from Fig. 24, the peak efficiency of the inverter under the CSFSPWM method is around 97.12% while it is about 97.48% under the PVSFSPWM method. In addition, the efficiency of the PVSFSPWM method is higher than that of the CSFSPWM method at the full power range. This is consistent with the theoretical analysis.

VI. Conclusion

This article proposed a PVSFSPWM method for harmonic spectrum improvement, filter inductor, and losses reduction. The implementation of the PVSFSPWM method is similar to the CSFSPWM method, and it does not have any closed-loop

operations, thus it is a passive method. By selecting the injection depth reasonably, the PVSFSPWM method has more advantages than CSFSPWM in the following aspects.

1) The PVSFSPWM method can effectively reduce the harmonic peak as well as EMI.
2) The PVSFSPWM method needs a smaller filter inductance than the CSFSPWM method under the same ripple current requirement.
3) The conduction losses for the two methods are the same, whereas the switching losses for the PVSFSPWM method are less than those for the CSFSPWM method.
4) The PVSFSPWM method is a passive method; better performances are obtained without closed-loop control.
5) The digital implementation of the PVSFSPWM method is the same as the traditional CSFSPWM method, which can generate gate signals by comparing sine wave and triangle wave. Therefore, no additional software overhead is required.

Because the injection depth has a huge impact on the system performance; the selection and optimization of injection depth will be carried out in future work carefully.

REFERENCES

[1] L. Vancini, M. Mengoni, G. Rizzoli, G. Sala, L. Zarri, and A. Tani, "Carrier-based PWM overmodulation strategies for five-phase inverters," *IEEE Trans. Power Electron.*, vol. 36, no. 6, pp. 6988–6999, Jun. 2021.

[2] H. Wang, L. Kou, Y. Liu, and P. Sen, "A seven-switch five-level active-neutral-point-clamped converter and its optimal modulation strategy," *IEEE Trans. Power Electron.*, vol. 32, no. 7, pp. 5146–5161, Jul. 2017.

[3] Y. Xia, K. Ahmed, and B. Williams, "A PWM current source-based DC transmission system for multiple wind turbine interfacing," *IEEE J. Emerg. Sel. Topics Power Electron.*, vol. 2, no. 4, pp. 784–796, Dec. 2014.

[4] M. Kumar and R. Gupta, "Sampling effect characterization of digital SPWM of VSI in time domain," *IEEE Trans. Ind. Electron.*, vol. 63, no. 7, pp. 4150–4159, Jul. 2016.

[5] Y. Zhang, Q. Li, and D. Jiang, "A motor CM impedance based transformerless active EMI filter for DC-side common-mode EMI suppression in motor drive system," *IEEE Trans. Power Electron.*, vol. 35, no. 10, pp. 10238–10248, Oct. 2020.

[6] F. Zhao, G. Xiao, T. Zhu, T. Zhao, X. Zheng, and Z. Wu, "Harmonic analysis and suppression method of output current distortion for medium-voltage motor drives with modular multilevel converter," *IEEE Trans. Power Electron.*, vol. 35, no. 1, pp. 744–759, Jan. 2020.

[7] R. Ramos, D. Serrano, P. Alou, J. Á. Oliver, and J. A. Cobos, "Control design of a single-phase inverter operating with multiple modulation strategies and variable switching frequency," *IEEE Trans. Power Electron.*, vol. 36, no. 2, pp. 2407–2419, Feb. 2021.

[8] J. Chen, D. Sha, J. Zhang, and X. Liao, "A variable switching frequency space vector modulation technique for zero-voltage switching in two parallel interleaved three-phase inverters," *IEEE Trans. Power Electron.*, vol. 34, no. 7, pp. 6388–6398, Jul. 2019.

[9] Z. Zhang, L. Wei, P. Yi, Y. Cui, P. Murthy, and A. Bazzi, "Conducted emissions suppression of active front end (AFE) drive based on random switching frequency PWM," *IEEE Trans. Ind. Appl.*, vol. 56, no. 6, pp. 6598–6607, Nov. 2020.

[10] K. Kim, Y. Jung, and Y. Lim, "A new hybrid random PWM scheme," *IEEE Trans. Power Electron.*, vol. 24, no. 1, pp. 192–200, Jan. 2009.

[11] M. Sharifzadeh, H. Vahedi, R. Portillo, L. Franquelo, and K. Al-Haddad, "Selective harmonic mitigation based self-elimination of triplen harmonics for single-phase five-level inverters," *IEEE Trans. Power Electron.*, vol. 34, no. 1, pp. 86–96, Jan. 2019.

[12] Y. Zhang, Y. Li, N. Zargari, and Z. Cheng, "Improved selective harmonics elimination scheme with online harmonic compensation for high-power PWM converters," *IEEE Trans. Power Electron.*, vol. 30, no. 7, pp. 3508–3517, Jul. 2015.

[13] Z. Yang, H. Li, F. Lin, B. Zhang, and J. Lü, "Common-mode electromagnetic interference calculation method for a PV inverter with chaotic SPWM," *IEEE Trans. Magn.*, vol. 51, no. 11, pp. 1–4, Nov. 2015.

[14] Z. Wang, K. T. Chau, and C. Liu, "Improvement of electromagnetic compatibility of motor drives using chaotic PWM," *IEEE Trans. Magn.*, vol. 43, no. 6, pp. 2612–2614, Jun. 2007.

[15] Y. Huang, Y. Xu, W. Zhang, and J. Zou, "Hybrid RPWM technique based on modified SVPWM to reduce the PWM acoustic noise," *IEEE Trans. Power Electron.*, vol. 34, no. 6, pp. 5667–5674, Jun. 2019.

[16] R. Gamoudi, D. Chariag, and L. Sbita, "A review of spread-spectrum-based PWM techniques—A novel fast digital implementation," *IEEE Trans. Power Electron.*, vol. 33, no. 12, pp. 10292–10307, Dec. 2018.

[17] F. Yu *et al.*, "Design and FPGA implementation of a pseudorandom number generator based on a four-wing memristive hyperchaotic system and Bernoulli map," *IEEE Access*, vol. 7, pp. 181884–181898, 2019.

[18] X. Mao, R. Ayyanar, and H. Krishnamurthy, "Optimal variable switching frequency scheme for reducing switching loss in single-phase inverters based on time-domain ripple analysis," *IEEE Trans. Power Electron.*, vol. 24, no. 4, pp. 991–1001, Apr. 2009.

[19] D. Jiang and F. Wang, "A general current ripple prediction method for the multiphase voltage source converter," *IEEE Trans. Power Electron.*, vol. 29, no. 6, pp. 2643–2648, Jun. 2014.

[20] Z. Wang, Z. Zhao, M. H. Uddin, and Y. Zhao, "Current ripple analysis and prediction for three-level T-type converters," in *Proc. IEEE Energy Convers. Congr. Expo.*, 2018, pp. 7251–7257.

[21] D. Jiang and F. Wang, "Variable switching frequency PWM for three-phase converters based on current ripple prediction," *IEEE Trans. Power Electron.*, vol. 28, no. 11, pp. 4951–4961, Nov. 2013.

[22] Q. Li and D. Jiang, "Variable switching frequency PWM strategy of two-level rectifier for DC-link voltage ripple control," *IEEE Trans. Power Electron.*, vol. 33, no. 8, pp. 7193–7202, Aug. 2018.

[23] O. Oñederra, I. Kortabarria, I. Alegría, J. Andreu, and J. Gárate, "Three-phase VSI optimal switching loss reduction using variable switching frequency," *IEEE Trans. Power Electron.*, vol. 32, no. 8, pp. 6570–6576, Aug. 2017.

[24] L. Wei and R. A. Lukaszewski, "Pulse width modulation (PWM) rectifier with variable switching frequency," U.S. Patent 7 190 143 132, Mar. 2007.

[25] A. Kumar and G. Narayanan, "Variable-switching frequency PWM technique for induction motor drive to spread acoustic noise spectrum with reduced current ripple," *IEEE Trans. Ind. Appl.*, vol. 52, no. 5, pp. 3927–3938, Sep./Oct. 2016.

[26] D. Ye *et al.*, "Variable switching sequence PWM strategy of dual three-phase machine drive for high-frequency current harmonic suppression," *IEEE Trans. Power Electron.*, vol. 35, no. 5, pp. 4984–4995, May 2020.

[27] Z. Wang, J. Chen, M. Cheng, and K. T. Chau, "Field-oriented control and direct torque control for paralleled VSIs fed PMSM drives with variable switching frequencies," *IEEE Trans. Power Electron.*, vol. 31, no. 3, pp. 2417–2428, Mar. 2016.

[28] D. G. Holmes and T. A. Lipo, *Pulse Width Modulation For Power Converters: Principles and Practice*. Hoboken, NJ, USA: Wiley, 2003.

[29] H. Li, Y. Liu, J. Lü, T. Zheng, and X. Yu, "Suppressing EMI in power converters via chaotic SPWM control based on spectrum analysis approach," *IEEE Trans. Ind. Electron.*, vol. 61, no. 11, pp. 6128–6137, Nov. 2014.

[30] Q. Li, J. Chen, and D. Jiang, "Periodic variation in the effect of switching frequency on the harmonics of power electronic converters," *Chin. J. Elect. Eng.*, vol. 6, no. 3, pp. 35–45, Sep. 2020.

Xiaonan Zhu (Student Member, IEEE) was born in Henan, China, in 1995. He received the B.S. degree in electrical engineering from the China University of Petroleum, Qingdao, China, in 2017. He is currently working toward the Ph.D. degree in power electronics with the College of Electrical and Information Engineering, Hunan University, Changsha, China.

His current research interests include the power converter design, analysis and modulation techniques, grid integration of renewable energy, and control algorithms in power electronics.

Hongliang Wang (Senior Member, IEEE) received the B.Sc. degree in electrical engineering from the Anhui University of Science and Technology, Huainan, China, in 2004, and the Ph.D. degree in electrical engineering from the Huazhong University of Science and Technology, Wuhan, China, in 2011.

From 2004 to 2005, he was an Electrical Engineer with Zhejiang Hengdian Thermal Power Plant. From 2011 to 2013, he was a Senior System Engineer with Sungrow Power Supply Company, Ltd. From 2013 to 2018, he was a Postdoctoral Fellow with Queen's University. Since 2018, he has been with Hunan University, Changsha, China, where he is currently a Full Professor with the College of Electrical and Information Engineering. He has authored more than 60 technical papers in journals and conferences. He is the inventor/co-inventor of 42 China-issued patents and 8 U.S.-issued patents. His current research interests include multilevel topology, high-gain topology, parallel technology and virtual synchronous generator technology for PV application and microgrids application, resonant converters and server power supplies, and LED drivers.

Dr. Wang is currently a Senior Member of China Electro-Technical Society (CES) and China Power Supply Society (CPSS). He is a member of CPSS Technical Committee on Standardization and CPSS Technical Committee on Renewable Energy Power Conversion, a China Expert Group Member of IEC Standard TC8/PT 62786, a Vice-Chair of IEEE Kingston Section, a Session Chair of 2015 IEEE Energy Conversion Congress and Exposition (ECCE) and ECCE 2017, and a TPC member of the 2012 International Conference on Electrical Machines and Systems.

Wenyuan Zhang received the M.Sc. degree in electrical engineering from Guangxi University, Nanning, China, in 2017. He is currently working toward the Ph.D. degree in electrical engineering with the College of Electrical and Information Engineering, Hunan University, Changsha, China.

From 2017 to 2019, he was an Electrical Engineer with CRRC Dalian R&D Company, Ltd. His current research interests include digital control techniques, modulation strategies, topology research of multilevel converters, and renewable energy systems.

Hanzhe Wang received the B.S. and M.S. degrees in electrical engineering from the China University of Mining and Technology, Xuzhou, China, in 2016 and 2019, respectively. He is currently working toward the Ph.D. degree in power electronics with Hunan University, Changsha, China.

His current research interests include digital control techniques, modulation strategies, multilevel topology of inverter for photovoltaic application, and renewable energy systems control.

Xiaojun Deng received the B.S. degree in electrical engineering from the China University of Mining and Technology, Xuzhou, China, in 2019. He is currently working toward the Ph.D. degree in power electronics with Hunan University, Changsha, China.

His research interests include power electronics, multilevel converters in renewable energy, and control algorithms.

Wei Tang received the B.S. degree in electrical engineering from Yanshan University, Qinhuangdao, China, in 2020. He is currently working toward the Ph.D. degree in power electronics with Hunan University, Changsha, China.

His research interests include LLC resonant converter, inverter topology and control, multilevel converter in renewable energy, and control algorithms.

Xiumei Yue received the B.Sc. degree from the Anhui University of Science and Technology, Huainan, China, in 2004, and the M.Sc. degree from the Huazhong University of Science and Technology, Wuhan, China, in 2007, both in electrical engineering.

From 2007 to 2011, she was with Hubei Polytechnic University. From 2011 to 2014, she was a Senior Intellectual Property Engineer with Sungrow Power Supply Company, Ltd. From 2014 to 2017, she was with Queen's University, Canada. Since 2018, she has been with Hunan University, Changsha, China. Her current research interests include converter topology and control technology, and dc/ac converter.